FABRY–PÉROT LINE PROFILES IN THE λ5303 Å AND λ6374 Å CORONAL LINES OBTAINED DURING THE 1983 INDONESIAN ECLIPSE

T. CHANDRASEKHAR, J. N. DESAI, N. M. ASHOK

Physical Research Laboratory, Ahmedabad, 380009, India

and

JAY M. PASACHOFF

Institute for Advanced Study, Princeton, NJ 08540, U.S.A.

and

Hopkins Observatory, Williams College, Williamstown, MA 01267, U.S.A.

(Received 24 April 1990; in revised form 2 August 1990)

Abstract. During the total solar eclipse of 11 June, 1983, an imaging dual-channel Fabry–Pérot interferometer was used to obtain line profiles simultaneously in the green λ5303 Å [Fe XIV] and the red λ6374 Å [Fe X] coronal lines at various positions in the corona. Extensive microdensitometry followed by multi-Gaussian curve-fitting analysis has resulted in the determination of coronal temperatures and velocity separations between different pockets of coronal gas in the line of sight over a large extent of the corona. Fewer high temperature zones are to be found in the corona of 1983 compared with our similar green-line measurements of the solar maximum corona of 1980. The data are consistent with a temperature maximum occurring at 1.2 $R_\odot$, as found at the 1980 eclipse, but our new data are insufficient to observe farther out than this radius and so determine the position of a maximum. The velocity field in the corona at the 1983 eclipse is less structured compared with that at the 1980 eclipse and is mainly confined to the zone 20–30 km s^{-1}.

1. Introduction

Imaging spectroscopy of coronal emission lines using Fabry–Pérot etalons is an elegant and powerful technique for obtaining simultaneously spectral line profiles at various positions in the emission corona during the short period of totality of a solar eclipse. The study of line profiles obtained from a Fabry–Pérot interferogram can be invaluable in

(a) determining the line widths and, hence, Doppler temperatures over the entire extent of the corona. The Doppler temperatures can be compared with the theoretical models of the coronal temperature structure,

(b) delineating the existing velocity fields in the corona from a measurement of Doppler shifts or through the decomposition of a complex profile into its constituent parts; and

(c) providing unambiguous evidence of mass flows in the corona from split fringes in the interferogram.

The spatially-resolved temperature and velocity field information also serve as useful inputs to the 3-dimensional modelling of complex coronal structures like loops.

Solar Physics **131:** 25–39, 1991.

In this paper we present the results of the line-profile analysis carried out in the green-line and red-line Fabry–Pérot interferograms obtained during the Indonesian total solar eclipse of 11 June, 1983.

2. Observations

The interferograms were obtained in the [Fe XIV] green line λ5303 Å and the [Fe X] red line λ6374 Å simultaneously during totality of the eclipse of 11 June, 1983, from Tanjung Kodak, Java, Indonesia. A dual-channel Fabry–Pérot interferometric system was specifically designed, fabricated and used to obtain the coronal interferograms. Details of the instrument and the observations made are given elsewhere (Chandrasekhar *et al.*, 1984). The green line was obtained in transmission and the red line was obtained in reflection, leading to the different orientations of the images reproduced in that paper.

3. Analysis

3.1. Microdensitometry

Extensive microdensitometry has been carried out on the two eclipse frames: (a) a green-line frame with exposure time of 3^m30^s and (b) a red-line frame with exposure time of 3^m40^s. A Carl Zeiss densitometer with a slit width of 80 microns, corresponding to 0.6″ in the sky, and a slit height of 48″ for both the frames was used to generate the scans. The scans were always taken radially to or from the fringe center. The fringe centers for both the frames were not coincident with the solar center. This off-axis mode of operation was specifically chosen in order to achieve near radial coverage of line profiles in coronal regions close to fringe center and closely spaced fringes in a direction diametrically opposite. The scanning slit width of 80 microns corresponds to a spectral resolution, in a typical region of the interferograms, of 0.09 Å (5303 Å) and 0.05 Å (6374 Å), which are both below the instrumental resolutions of 0.33 Å (5303 Å) and 0.23 Å (6374 Å). Hence, there is no loss of spectral resolution in microdensitometric scanning. The spatial resolution – the interfringe distance – is variable across the interferogram because of the off-axis operation. However, in a typical region of the interferograms, the resolution is $\sim 0.03\ R_\odot$ (0.45 arc min) for the green line and $0.05\ R_\odot$ (0.75 arc min) for the red line.

The radial microdensitometric data were obtained on a chart that was then read and manually digitized. The digitized density values were then converted to relative intensities using the film characteristic curves derived from the step-wedge calibration impressed on the film.

Our profiles extended only up to about $1.25\ R_\odot$ in the 3^m30^s exposure at the 1983 eclipse, less than the $1.5\ R_\odot$ we obtained in the green line at the 1980 eclipse in a 90^s exposure. This can be explained in part by our use of Kodak 2415 film in 1983 because of its finer grain, compared with the faster Kodak Tri-X we used in 1980. Also, we had a beamsplitter with 50% transmission in our 1983 system. Furthermore, we observed

through clouds in 1983 compared with a clear sky in 1980. Finally, because of the solar cycle, the 1983 eclipse corona was dimmer than the 1980 corona.

3.2. Line profile generation

In each microdensitometric scan radially through the fringe center, one or more fringes are encountered. The number of fringes depends on the portion of the corona scanned. The positions of various points on each fringe relative to the center of the fringe pattern were carefully measured. Using the Fabry–Pérot expression, valid for small angles of incidence θ, we have for any point on a fringe

$$\theta\,\Delta\theta \sim \frac{R(R - R_\odot)}{F^2} \sim \frac{\Delta\lambda}{\lambda_0} \sim \frac{\lambda - \lambda_0}{\lambda_0}\,,$$

where R is the radius measured from the fringe center, $R_\odot$ is the radius of fringe peak corresponding to wavelength λ_0, and F is the focal length of the camera lens.

From the above $\Delta\lambda$, the wavelength separation from the fringe peak was determined. This procedure was carried out for all the fringes. The relative intensity values together with $\Delta\lambda$ for each fringe determine the spectral line profile.

We selected for analysis 53 green-line (λ5303 Å) profiles extending up to a maximum extent of 1.23 $R_\odot$ from the solar center, chosen for their good signal-to-noise ratio (> 20) out of 196 profiles measured. The selected red-line (λ6374 Å) profiles number 31 and extend up to 1.20 $R_\odot$.

3.3. Multi-Gaussian analysis

A multi-Gaussian curve-fitting program was carried out on each of the profiles generated. Each profile was compared with a single, double, or triple Gaussian:

$$I(X) = \sum A_i \exp\left[- \left(\frac{X - X_i}{a_i} \right)^2 \right], \quad i = 1, 2, 3\,.$$

The parameters of the best profile were then determined. The multi-Gaussian fits have survived testing for sensitivity of starting parameters. Table I gives the results of the multi-Gaussian analysis.

Almost half the 53 green-line profiles are best fit by a single Gaussian. Double-Gaussian best fits are also common, while triple-Gaussian best fits are rare. Most of the line profiles thus require only one or two Gaussian components for a good fit. Six fringes do not fall into any of these categories and have been classified as ambiguous. We thus do not include them in the analysis.

The red-line profiles have a larger continuum contribution. We thus consider the green-line profiles for most of our analysis.

3.4. Determination of temperature and relative velocity

The analysis results in the determination of the amplitude, position of the peak, and the Gaussian width of each of the components. The individual Gaussian widths ($\Delta\lambda_D$) are

TABLE I

Multi-Gaussian fits for profiles

Best fit profiles	No. of profiles	
	5303 Å green line	6374 Å red line
Single Gaussian	25	18
Double Gaussian	19	3
Triple Gaussian	2	0
Ambiguous	7	10
Total	53	31

corrected for instrumental broadening amounting to 0.33 Å in the green-line interferogram and the line-width temperature (T) determined from the expressions

$$\Delta\lambda_D^2 = (4 \ln 2) a_1^2 ,$$

$$(\Delta\lambda_D^2)_{\text{corr}} = \Delta\lambda_D^2 - (0.33)^2 ,$$

$$(\Delta\lambda_D)_{\text{corr}} = 7.16 \times 10^7 \sqrt{\frac{T}{m}} ,$$

where $(\Delta\lambda_D)_{\text{corr}}$ is the corrected width of a Gaussian component and m is the mass number of the emitting atom (56 for iron, in this case).

For the case of a double-Gaussian best fit, in addition to the line-width temperatures the velocity separation between the component profiles V_{12} can be determined by

$$V_{12} = \frac{c(X_1 - X_2)}{\lambda_0} ,$$

where $\lambda_0 = 5303$ Å. We derive one relative velocity for each of the 19 double Gaussians and two each for both triple Gaussians, for a total of 23 relative-velocity measurements.

The accuracy of the measurements of temperature line-width and relative velocity determination are listed in Table II.

The main source of noise in the interferogram is the grain noise caused by the film, which limits the accuracy of measurement of half-width points of the line profiles. For profiles with very good signal-to-noise ratios ($S/N \gtrsim 20$), the line widths can be

TABLE II

Accuracy of measurements

Line-width	$\pm 5\%$ to $\geq 10\%$
Temperature	$\pm 10\%$ to $\geq 20\%$
Typical spatial resolution	$\sim 0.03 R_\odot$ for green interferogram
	$\sim 0.05 R_\odot$ for red interferogram
Relative velocity resolution	± 5 km s^{-1}

measured to within 5%, while moderately good profiles ($S/N \sim 10$) have line-width accuracies nearer 10%.

In the analysis, we selected only the 53 green-line profiles that exhibited good signal-to-noise ratios ($S/N \gtrsim 10$) out of a total available data set of 196 green-line measurements. Of these 53 profiles, as many as 25 are best fitted by a single Gaussian. In the single-Gaussian analysis, the line width and amplitude are independently varied and the value (observed − calculated)^2 minimized for best fit. The index of correlation, which is a measure of the goodness of fit, ranges from 0.93 to 0.99, indicating a good fit to the Gaussian profile. In the multi-Gaussian analysis, the separation between Gaussian peaks is another parameter that is independently varied in obtaining the best fit. The Gaussian fits to the data are quite sensitive, and errors involved in fitting are much less than those involved in the microdensitometric reduction of the profile, such as limitation from grain noise, errors involved in intensity calibration, etc. Hence, the line-width measurements are limited by grain noise to the accuracies given in Table II. The case of small line widths ($\Delta\lambda < 0.6$ Å) involves another factor, which is discussed below.

In the analysis, we correct the Gaussian profile fitted to the data for instrumental broadening (instrumental width = 0.33 Å for the green line) to obtain the line width and, hence, the line-width temperature. Smaller line widths ($\Delta\lambda < 0.6$ Å) are more sensitive to the deconvolution of the instrumental profile from the fitted Gaussian profile to the data. The instrumental profile is an Airy profile convolved with the plate-flatness profile of the Fabry–Pérot etalon. Then the exact nature of the instrumental profile becomes increasingly important, especially in the wings of the line. There are three values of low line widths in our single-Gaussian green-line data (A331, A031, and A442) that need to be treated with some caution.

4. Results

4.1. Line-width temperatures

4.1.1. *Green-Line Temperature*

Line-width Doppler temperatures obtained from the green-line profiles peak in the $(2–3) \times 10^6$ K region. During the Indian eclipse of 1980, a similar experiment was carried out by the authors (Chandrasekhar, Desai, and Angreji, 1981; Desai and Chandrasekhar, 1983), limited to the green line. The histograms of single-Gaussian λ5303 Å line-width temperatures for the 1980 and 1983 eclipses are shown in Figure 1. While the line-width temperatures were sharply confined to the zone $(2–3) \times 10^6$ K during the 1983 eclipse, many regions had recorded line-width temperatures in excess of 3×10^6 K during the eclipse in the solar maximum year 1980. Statistically, at the 1980 eclipse, 35% of all the recorded line-width temperatures were in excess of 3×10^6 K, while at the 1983 eclipse that figure was only 24%.

Figure 2 shows the distribution of single-Gaussian Doppler temperatures of the green

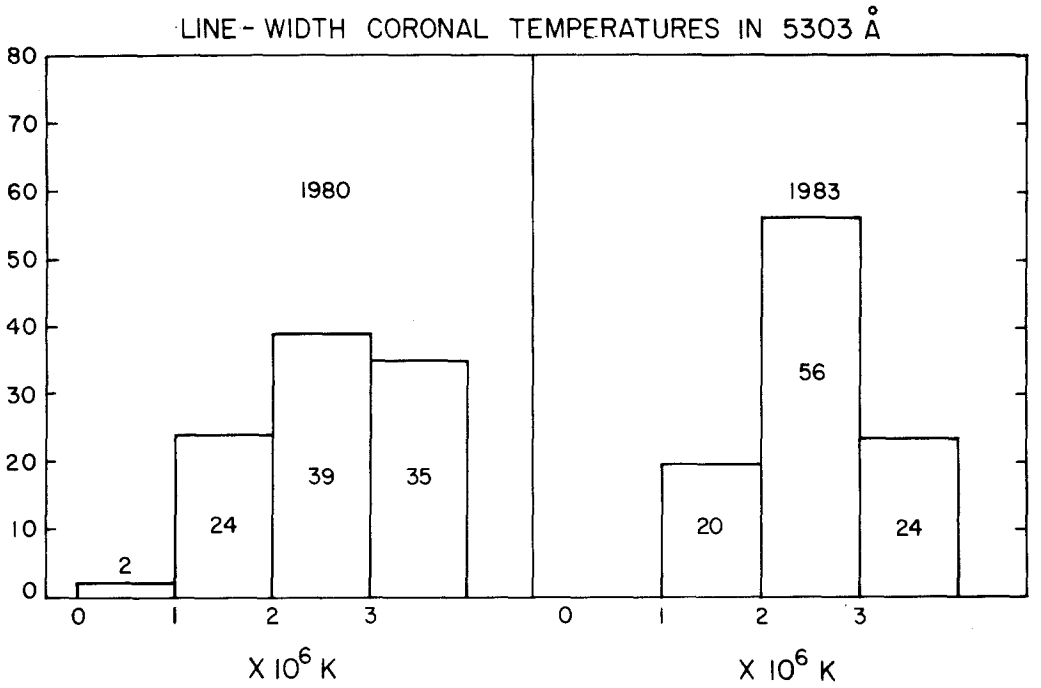

Fig. 1. A histogram showing the percentages of green-line coronal line-width temperatures in different intervals for the 1980 solar maximum and 1983 decaying-cycle eclipses. Temperature values of 1, 2, 3, and 4×10^6 K correspond to $\Delta\lambda_D = 0.304$, 0.430, 0.527, and 0.608 Å, respectively.

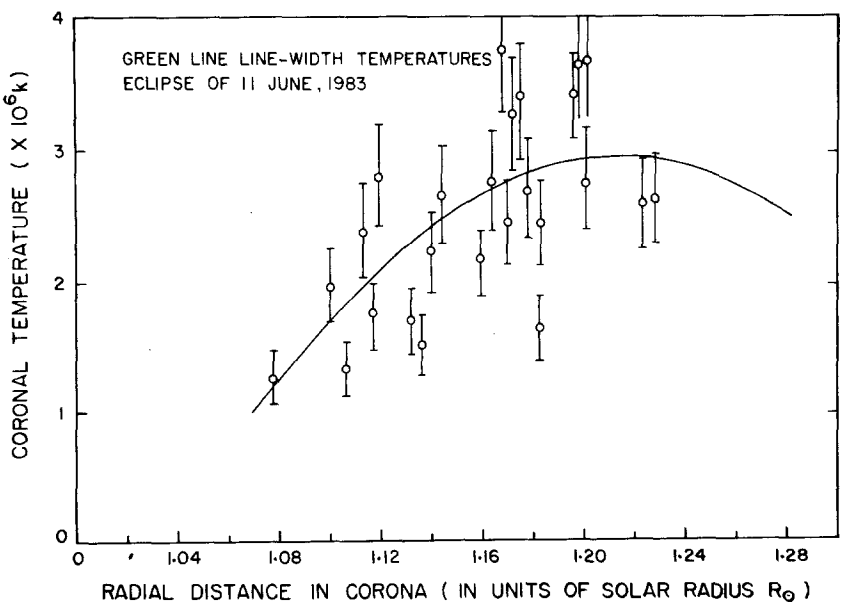

Fig. 2. A plot of green-line coronal line-width temperature against radial distance in the corona measured in units of solar radius. The curve is a least-squares fit.

line as a function of radial distance ($R/R_\odot$). The values indicate a rise to a maximum in the region 1.18–1.20 $R_\odot$ and then a tendency to fall off with higher radial distance. Paucity of data beyond 1.22 $R_\odot$ makes it difficult to show a clear drop-off after the maximum. A least-square fit to the data is represented by the curve in Figure 2, which has a maximum at 1.21 $R_\odot$. It may be noted that during the 1980 eclipse, observations were available up to 1.5 $R_\odot$ at most position angles and profiles showed a peak line-width temperature at 1.2 ± 0.05 $R_\odot$. Thus green-line observations at both the 1980 and 1983 eclipses are consistent with a peak line-width temperature at about the same distance (1.2 $R_\odot$) from the solar centre.

4.1.2. *Red-Line Temperatures*

Figure 3 shows the histogram of the red-line (6374 Å) line width temperatures. Here again we find that the line-width temperatures are confined mainly to the region $(2–3) \times 10^6$ K.

Figure 4 shows the radial variation of red line-width temperatures. The data clearly show a rise in temperature at least up to 1.18 $R_\odot$. There are no data much beyond 1.2 $R_\odot$ from our observations and hence it is not possible to reach any conclusions on the line-width temperature maximum. The least-square curve fitted to the available data also does not exhibit any maxima.

4.2. Relative Velocity

The line profiles that are fitted best by a double (or triple) Gaussian clearly indicate in the line of sight two (or three) pockets of coronal gas that are moving relative to one another. The relative velocity between the components can be deduced from the interferograms. The relative velocities in the green line at the 1980 and 1983 eclipses are compared in a histogram (Figure 5).

The 1980 green-line corona exhibited rather large velocities. There was even a region (position angle 256°) in the 1980 interferogram that showed fringe splitting, implying a well-defined relative motion at that position in the corona to the extent of ~ 70 km s^{-1} (Chandrasekhar, Desai, and Angreji, 1981).

The relative velocity values in 1983 are comparatively small. A majority of the velocities are confined to the region 20–30 km s^{-1}. About one-fifth of the velocities measured are in the 10–20 km s^{-1} region. The method of deconvolving a complex line profile into its individual Gaussian components is insensitive to Gaussians whose peaks are separated by small values of relative velocity (< 10 km s^{-1}). Hence, the lack of relative velocities in the 1–10 km s^{-1} region is likely to be an observational limitation. A few single Gaussian profiles could perhaps be interpreted in terms of double Gaussian profiles separated by small relative velocities. However, it is clear from the analysis that large velocities, in excess of 30 km s^{-1}, were definitely not as prevalent in 1983 as in 1980.

Figure 6 shows the plots of coronal line-width temperature and the relative velocities plotted against position angle. Our measurements were only of adequate signal-to-noise in two zones, one centered around 80° and the other around 230°. The orientation was

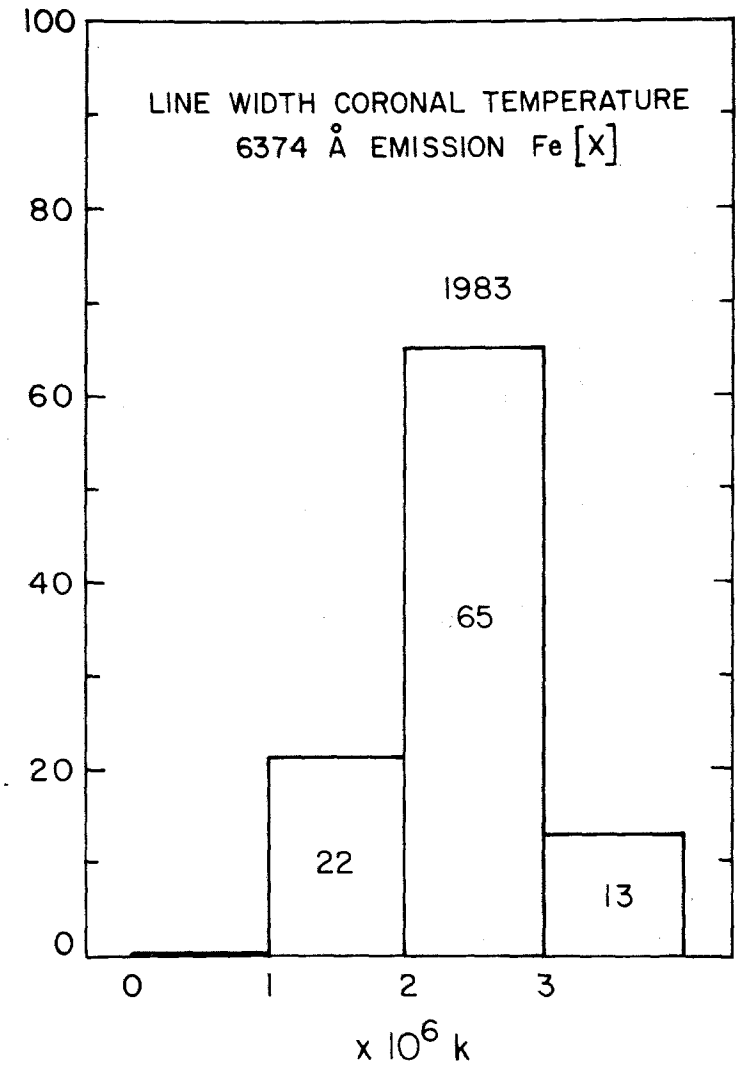

Fig. 3. A histogram showing percentages of red-line coronal line-width temperatures in different intervals for the 1983 eclipse. Temperature values of 1, 2, 3, and 4 × 10^6 K correspond to $\Delta\lambda_D$ = 0.365, 0.517, 0.633, and 0.737 Å, respectively.

derived from the third contact point as given in U.S. Naval Observatory Circular 165, and should be accurate to ± 2°. At intermediate positions, the green-line intensities are weaker and line profiles are too ill-defined to draw definitive conclusions, though our azimuthal coverage was complete when all the measured profiles are considered.

The red-line profiles are mostly fitted by single Gaussians. Three profiles, however, need a double Gaussian with relative velocities in the region 25–30 km s^{-1}. Interestingly, two of these profiles are in the position-angle region 97–100°, in which green-line velocities of the same order are also available.

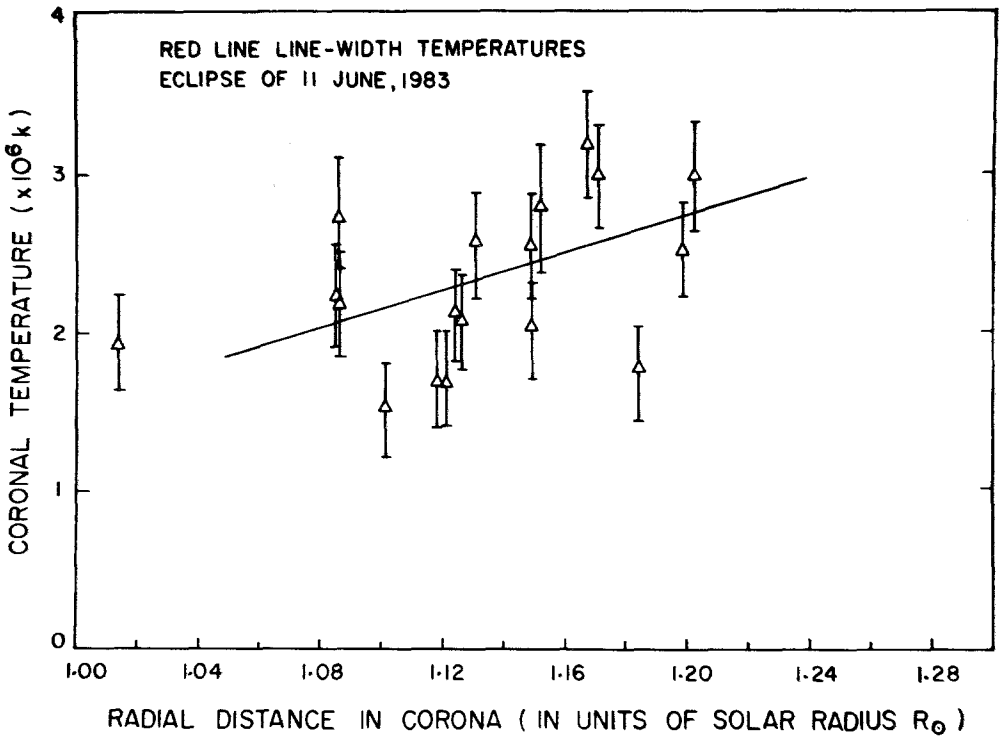

Fig. 4. A plot of red-line coronal line-width temperature against radial distance in the corona measured in units of solar radius. The curve is a least-squares fit.

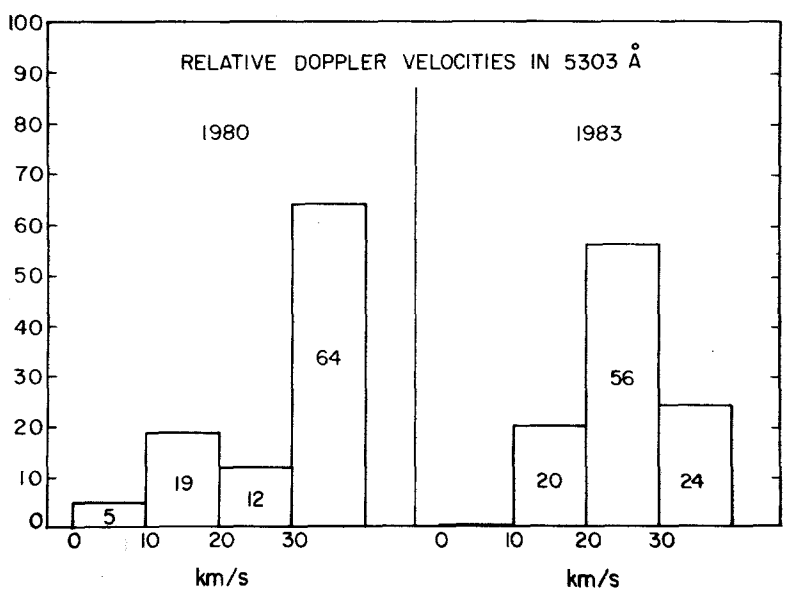

Fig. 5. A histogram showing the percentages of relative Doppler velocities in different ranges derived from green-line profiles for the 1980 and 1983 eclipses.

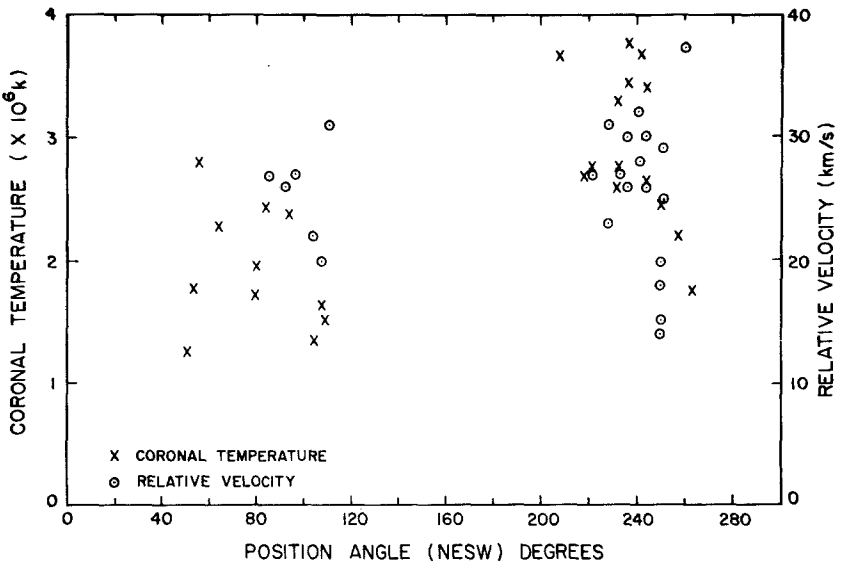

Fig. 6. A plot of coronal line-width temperature and relative Doppler velocity in the green line against position angle in the corona of 11 June, 1983.

Comparison with a white-light coronal map (Loucif and Koutchmy, 1989) shows that one of the zones of visibility corresponds to one of the two major streamers on the Sun, but that no special profiles correspond to the other major streamer. Our results are at altitudes $< 1.2\, R_\odot$; the streamer we have detected appears bright at such low altitudes while the other streamer appears bright only for altitudes $> 1.3\, R_\odot$. The green-line intensities for 1.15, 1.35, and 1.45 R_0 are given from Sacramento Peak Observatory 5303 Å data in *Solar-Geophysical Data* for 11 June, 1983, 15:15:23 UT, 11 hours after the 04:33 UT eclipse. The other zone of visibility in our data corresponds to a region of small equatorial streamers. The high-velocity profiles also correspond to only small equatorial streamers. We have confirmed these correspondences with the High Altitude Observatory radial-coronagraph image (Fisher, Bauer, and Lacey, 1983; Sime *et al.*, 1984).

4.3. Turbulent Velocities

The preceding analysis has derived line-width temperatures from the observed line widths for single-Gaussian profiles. The question of microturbulent velocities, as always, is worthy of detailed consideration. For the 1980 solar eclipse (Desai and Chandrasekhar, 1983), we derived turbulent velocities at many places in the corona using the observed line-width temperatures, the ratio of line intensity to the square of the continuum intensity, and the ionization equilibrium calculations discussed by Jordan (1969). Unfortunately, for the 1983 Indonesian eclipse, the images were too weak to properly register the continuum intensity between the fringes, so we could not derive turbulent velocities in this way.

Tables III and IV show both the line-width temperature derived from the assumption of turbulent velocity $\xi = 0$ and the turbulent velocity ξ derived for the temperatures of

TABLE III

Turbulent velocities from λ5303 Å single-Gaussian line profiles

Scan No.	Profile ident.	R/R_0	P.A. (°)	Line width FWHM (Å)	T_{eff} ($\times 10^6$ K) if $\xi_G = 0$	ξ_G (km s^{-1}) for $T = 1.8 \times 10^6$ K
1	A331	1.077	50.5	0.572	1.27	–
2	A341	1.117	52.5	0.674	1.76	–
3	A351	1.119	55.6	0.849	2.80	17
4	A361	1.114	63.8	0.759	2.24	12
5	A381	1.132	78.9	0.665	1.72	–
6	A391	1.100	80.0	0.710	1.96	7
7	A392	1.183	83.8	0.792	2.44	14
8	A421	1.113	93.5	0.783	2.38	13
9	A031	1.116	105.4	0.590	1.35	–
10	A432	1.183	106.1	0.650	1.64	–
11	A442	1.136	108.7	0.626	1.52	–
12	A112	1.198	206.8	0.968	3.64	23
13	A131	1.178	217.3	0.861	2.88	18
14	A141	1.164	221.8	0.842	2.76	17
15	A162	1.172	232.6	0.918	3.28	21
16	A163	1.201	232.6	0.843	2.76	17
17	A172	1.167	236.4	0.982	3.75	24
18	A173	1.196	236.4	0.940	3.43	22
19	A174	1.224	236.4	0.817	2.60	16
20	A184	1.201	241.0	0.971	3.67	24
21	A193	1.175	243.6	0.938	3.41	22
22	A195	1.228	243.5	0.824	2.64	16
23	A203	1.170	249.7	0.795	2.46	14
24	A222	1.159	256.8	0.750	2.19	11

maximum abundance, which are 1.8×10^6 K for Fe XIV ions and 1.0×10^6 for Fe X ions (Jordan, 1969). The lines are too narrow in some cases to derive ξ. The half-width $\Delta\lambda$ listed is the full-width at half-maximum, which is related to the temperature of maximum abundance $T_{\max}$ and turbulent velocity ξ by

$$\left(\frac{\Delta\lambda}{\lambda}\right)^2 = \frac{4 \ln 2}{c^2}\left(\frac{2kT_{\max}}{m_{\text{Fe}}} + \xi^2\right).$$

For 5303 Å,

$$\xi_G = \sqrt{3.246 \times 10^{20}\left(\frac{\Delta\lambda}{\lambda}\right)^2 - 5.317 \times 10^{12}} \quad \text{cm s}^{-1}.$$

For 6374 Å,

$$\xi_R = \sqrt{3.246 \times 10^{20}\left(\frac{\Delta\lambda}{\lambda}\right)^2 - 2.954 \times 10^{12}} \quad \text{cm s}^{-1}.$$

TABLE IV

Turbulent velocities from λ6374 Å single-Gaussian line profiles

Scan No.	Profile ident.	R/R_0	P.A. (°)	Line width FWHM (Å)	T_{eff} ($\times 10^6$ K) if $\xi_R = 0$	ξ_R (km s^{-1}) for $T = 1.8 \times 10^6$ K
1	B081	1.132	1.5	0.974	2.55	22
2	B072	1.185	4.8	0.808	1.76	15
3	B071	1.125	7.2	0.885	2.11	18
4	B062	1.150	14.3	0.967	2.52	21
5	B061	1.087	17.4	1.005	2.71	23
6	B041	1.125	18.8	0.781	1.64	14
7	B211	1.086	32.7	0.907	2.21	19
8	B031	1.014	38.8	0.802	1.73	15
9	B191	1.087	42.4	0.896	2.16	19
10	B182	1.122	46.0	0.791	1.68	14
11	B121	1.169	341.1	1.087	3.17	26
12	B113	1.204	342.8	1.055	2.99	24
13	B112	1.153	344.3	1.019	2.79	23
14	B111	1.102	346.0	0.757	1.54	13
15	B102	1.172	348.4	1.051	2.97	24
16	B101	1.127	349.9	0.877	2.07	18
17	B092	1.200	353.6	0.961	2.49	21
18	B091	1.150	355.4	0.870	2.03	18

Turbulent velocities are shown in Figure 7. In the green line, most of the turbulent velocities are in the 10–20 km s^{-1} range (63% of the total); 32% fall in the 20–30 km s^{-1} range, and only 5% of the velocities fall in the range 0–10 km s^{-1}. The

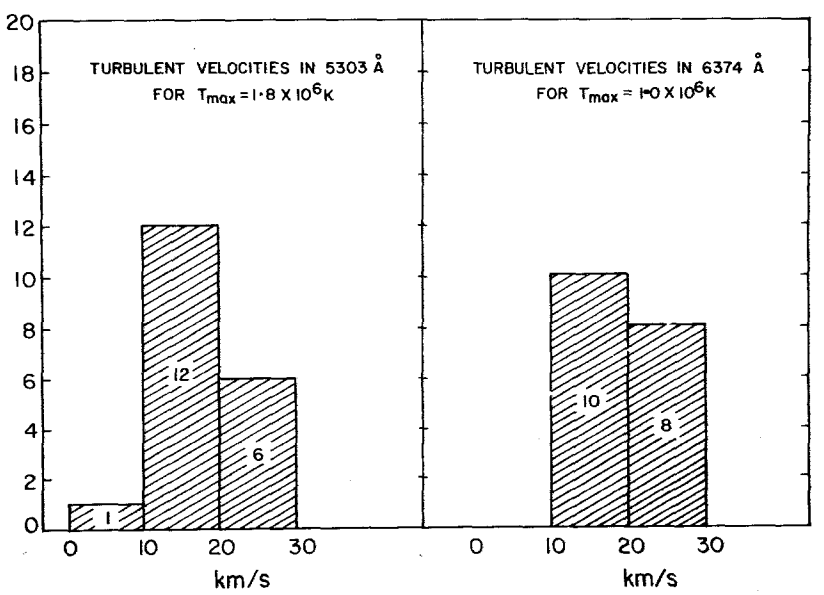

Fig. 7. Histogram showing the number of turbulent velocities in different ranges derived from single-Gaussian profiles measured at the 1983 total eclipse.

larger turbulent velocities (> 20 km s^{-1}) are in the vicinity of the streamer (position angle 230°–240°). No very large turbulent velocities (> 30 km s^{-1}) are found. In the red line, 56% of the values are in the 10–20 km s^{-1} range while the rest are in the 20–30 km s^{-1} range, but the result is not statistically different from the result for the green line. The red-line values seem generally larger in the position angle 340°–350°, which is close to the rotational pole and where a coronal hole shows (Sime *et al.*, 1984).

In Figure 8, we plot the turbulent velocity for both the lines as a function of the radial distance $R/R_\odot$ (ignoring the position angles). The turbulent velocity appears to increase

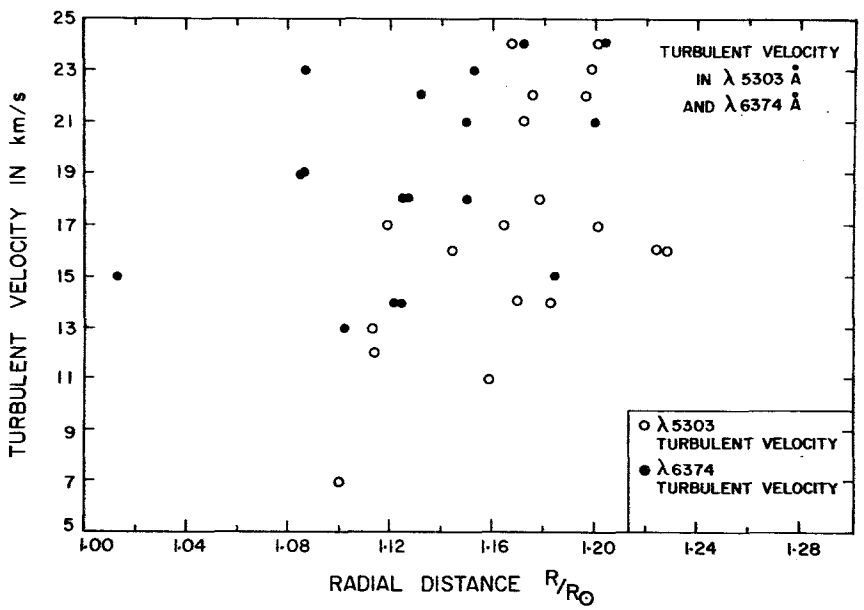

Fig. 8. Derived turbulent velocities vs radial distance for the single-Gaussian profiles measured at the 1983 total eclipse.

somewhat with height, but we cannot say whether this is a real effect or if it was brought about by assuming the temperature to be constant for each ion.

4.4. Future observations

The relative velocities in the corona we found at the 1980 and 1983 solar eclipses are not comparable with the similar velocities found by Delone and Makarova (1969) from their Fabry-Pérot studies through clouds of the 30 May, 1965, eclipse, for we measured relative velocities within individual profiles while they measured the deviation of the maximum intensities of their 6374 Å profiles from the positions expected from their interferometer spacing as calculated from krypton lines photographed before and after totality. Such large velocities were not found in the multi-slit studies of Livingston and Harvey (1982). Causes for the difference could include the selection of regions observed or the interpretation of the Fabry–Pérot profiles, though solutions invoking more turbulent velocity instead of two-Gaussian and three-Gaussian fits clearly agreed less

well with our data. It would not be unexpected to detect the result of inhomogeneous coronal velocity fields; one coronal region was seen even in white light at the solar-maximum 1980 eclipse to change its morphological structure drastically during the interval that the lunar shadow took to travel from African to Indian sites. Coronal X-ray observations show the breakup of the corona at 2 arc sec resolution to small-scale structure.

If differential motion were to continue at 10 km s^{-1} for the over 4 min scheduled for the next solar-maximum eclipse, which will occur on Mauna Kea and on other parts of the island of Hawaii on 11 July, 1991, it would correspond to 2500 km or 3 arc sec on the Sun. Thus velocities of 20 m s^{-1} or larger could show as displacements during high-resolution spectral-line imaging of the corona during totality. Suitable regions, however, must be chosen. Since the eclipse is to pass Hawaii at 17:30 UT, Baja California at 18:50 UT, and Brazil at 20:40 UT, the velocity of 10 km s^{-1} (36 000 km hr^{-1} = 1 arc min hr^{-1}) could give readily detectable differences to a series of identical cameras with green-line or red-line filters spaced along the eclipse path. Further Fabry–Pérot observations would also be expected to again show the relative high velocity dispersions at this solar-maximum eclipse. Coupling the Fabry–Pérot to an image intensifier (Chandrasekhar *et al.*, 1988) would increase the spatial coverage of the corona. We cannot overemphasize the need, at future total eclipses, of obtaining well-exposed interferograms of the corona with as much azimuthal coverage as possible.

Acknowledgements

We thank Zadig Mouradian of l'Observatoire de Paris at Meudon and Serge Koutchmy of l'Institut d'Astrophysique, Paris, for their comments and suggestions.

The Indian authors would like to thank Prof. K. R. Sivaraman of the Indian Institute of Astrophysics, Bangalore, for his encouragement and support, particularly for the loan of a coelostat for the experiment. Financial support for the project came from the Department of Space, Government of India.

JMP's participation was supported by grants PRM-8114631 and RII-8304403 from the U.S. National Science Foundation, by NSF travel support through a grant to the National Center for Atmospheric Research from the National Science Foundation, and by a grant from the National Geographic Society. Completion of the paper was supported by NSF grant ATM-9005194. His work was also supported by a Division III Research Grant at the Bronfman Science Center of Williams College. He is grateful to Jean Audouze and l'Institut d'Astrophysique, Paris, for their hospitality during a sabbatical leave. He thanks John N. Bahcall and the Institute for Advanced Study, Princeton, for their hospitality and support during the completion of this paper.

References

Chandrasekhar, T., Desai, J. N., and Angreji, P. D.: 1981, *Appl. Opt.* **20**, 2172.
Chandrasekhar, T., Ashok, N. M., Pasachoff, Jay, M., and Sivaraman, K. R.: 1984, *Appl. Opt.* **23**, 508.
Chandrasekhar, T., Ashok, N. M., Debiprasad, C., and Desai, J. N.: 1988, *Opt. Eng.* **27**, 67–70.

Delone, A. B. and Makarova, E. A.: 1969, *Solar Phys.* **9**, 116.
Desai, J. N. and Chandrasekhar, T.: 1983, *J. Astrophys. Astron. (India)* **4**, 65.
Fisher, R. R., Bauer, T., and Lacey, L.: 1983, photograph, High Altitude Observatory of the National Center for Atmospheric Research; 1989: printed in Pasachoff, Jay M., *Contemporary Astronomy*, 4th ed., Philadelphia, Saunders College Publishing, p. 136.
Jordan, C.: 1969, *Monthly Notices Roy. Astron. Soc.* **142**, 501.
Livingston, W. C. and Harvey, J. W.: 1982, *Proc. Indian Nat. Acad.*, Suppl. No. 3, p. 18.
Loucif, M. L., and Koutchmy, S.: 1989, *Astron. Astrophys. Suppl. Ser.* **77**, 45.
Sime, D. G., Fisher, R. R., McCabe, M. K., and Mickey, D. L.: 1984, *Astrophys. J.* **278**, L123.